

Redox Behavior of Thermally Aged Ceria–Zirconia Mixed Oxides. Role of Their Surface and Bulk Structural Properties

María Pilar Yeste, Juan Carlos Hernández, Serafín Bernal,* Ginesa Blanco, José J. Calvino, José A. Pérez-Omil, and José M. Pintado

Departamento de Ciencia de los Materiales e Ingeniería Metalúrgica y Química Inorgánica, Facultad de Ciencias, Universidad de Cádiz, Campus Río San Pedro, E-11510 Puerto Real (Cádiz), Spain

Received March 16, 2006. Revised Manuscript Received April 7, 2006

The relationship existing between aging conditions, redox behavior, and surface/bulk structural properties of two thermally aged ceria–zirconia mixed oxides, CZ-MO and CZ-SO, is analyzed. The samples were prepared by applying to a fresh $\text{Ce}_{0.62}\text{Zr}_{0.38}\text{O}_2$ mixed oxide two alternative aging routines consisting of a reduction with H_2 at 1223 K (5 h), followed by either a mild, CZ-MO, or severe, CZ-SO, re-oxidation treatment. By combining high-resolution electron microscopy and a number of chemical characterization techniques, it is shown that the nanostructure of the aged oxides, specifically the total amount and surface presence of the phase exhibiting an ordered cationic sublattice (κ -like phase), is a key factor in determining their redox response. In the low-temperature reduction range ($T_{\text{redn}} \leq 773$ K), the enhanced reducibility of the CZ-MO sample is proposed to be kinetically controlled by its surface structure mainly consisting of the κ -like phase. In accordance with the reported results, the surface activation of the H_2 molecule, much faster on the CZ-MO sample, is proposed to be the rate controlling step of the overall reduction process. This proposal was further confirmed by the dramatic downward shift observed in the temperature-programmed reduction diagrams recorded for the corresponding oxide-supported rhodium samples. By contrast, in the high-temperature reduction range ($T_{\text{redn}} \geq 973$ K), the observed difference of reducibility, higher in the case of the CZ-MO sample, is interpreted as due to thermodynamic factors related to the nature of the predominant cationic sublattice structure, ordered for CZ-MO and disordered in the case of the CZ-SO sample.

Introduction

Ceria–zirconia mixed oxides are known to be very interesting catalytic materials. They have successfully replaced pure ceria as oxygen buffers in the latest generations of three-way auto-exhaust catalysts.^{1–3} Likewise, they are being increasingly investigated as a component of the catalytic materials used in hydrogen production reformers.^{4–7}

One of the most challenging aspects in the behavior of these materials is their chemical and structural sensitivity to thermal aging. It is presently well-established that the re-oxidation temperature applied to heavily reduced ceria–zirconia samples may reversibly modify their redox response.^{8–13} As shown in ref 10, successive redox cycles

consisting of reduction in a flow of 5% H_2/Ar , at 1223 K (1 h), followed by re-oxidation in a flow of 5% O_2/He , for 1 h, at either 873 or 1173 K, lead respectively to oxide samples with enhanced and deteriorated low-temperature reducibility. Likewise, it is experimentally well-supported that, in parallel with these chemical effects, significant changes do also occur in the oxide structure.^{8,9,12–17} In accordance with the available Raman spectroscopy,^{9,13,14} X-ray diffraction,^{8,9,13} and electron microscopy^{15–17} studies, it is generally assumed that by starting from a fresh ceria–zirconia sample typically exhibiting random distribution in its cationic sublattice, the high-temperature reduction treatment induces some ordering in the Ce and Zr distribution, thus resulting a pyrochlore-like structure. If this heavily reduced sample is re-oxidized at moderate temperatures ($T_{\text{reoxn}} \leq 873$ K), the cationic sub-

* Corresponding author. E-mail: serafin.bernal@uca.es.

- (1) Trovarelli, A., Ed. *Catalysis by Ceria and Related Materials*; Imperial College Press: London, 2002.
- (2) Di Monte, R.; Kaspar, J. *J. Mater. Chem.* **2005**, *15*, 633.
- (3) Di Monte, R.; Kaspar, J. *Topics Catal.* **2004**, *28*, 47.
- (4) Villegas, L.; Guilhaume, N.; Provendier, H.; Daniel, C.; Masset, F.; Mirodatos, C. *Appl. Catal., A* **2005**, *281*, 75.
- (5) Woosch, A.; Descorme, C.; Duprez, D. *J. Catal.* **2004**, *225*, 259.
- (6) Kusakabe, K.; Sotowa, K.; Eda, T.; Iwamoto, Y. *Fuel Process. Technol.* **2004**, *86*, 319.
- (7) Mattos, L. V.; de Oliveira, E. R.; Resende, P. D.; Noronha, F. B.; Passos, F. B. *Catal. Today* **2002**, *77*, 245.
- (8) Izu, N.; Omata, T.; Otsuka-Yao-Matsuo, S. *J. Alloys Compd.* **1998**, *270*, 107.
- (9) Otsuka-Yao-Matsuo, S.; Omata, T.; Izu, N.; Kishimoto, H. *J. Solid State Chem.* **1998**, *138*, 47.
- (10) Baker, R. T.; Bernal, S.; Blanco, G.; Cordon, A. M.; Pintado, J. M.; Rodríguez-Izquierdo, J. M.; Fally, F.; Perrichon, V. *Chem. Commun.* **1999**, 149.

- (11) Fornasiero, P.; Montini, T.; Graziani, M.; Kaspar, J.; Hungria, A. B.; Martínez-Arias, A.; Conesa, J. C. *Phys. Chem. Chem. Phys.* **2002**, *4*, 149.
- (12) Suda, A.; Ukyo, Y.; Yamamura, K.; Sobukawa, H.; Sasaki, T.; Nagai, Y.; Tanabe, T.; Sugiura, M. *J. Ceram. Soc. Jpn.* **2004**, *112*, 586.
- (13) Montini, T.; Hickey, N.; Fornasiero, P.; Graziani, M.; Bañares, M. A.; Martínez-Huerta, M. V.; Alessandri, I.; Depero, L. E. *Chem. Mater.* **2005**, *17*, 1157.
- (14) Montini, T.; Bañares, M. A.; Hickey, N.; Di Monte, R.; Fornasiero, P.; Kaspar, J.; Graziani, M. *Phys. Chem. Chem. Phys.* **2004**, *6*, 1.
- (15) Pérez-Omil, J. A.; Bernal, S.; Calvino, J. J.; Hernández, J. C.; Mira, C.; Rodríguez-Luque, M. P.; Erni, R.; Browning, N. D. *Chem. Mater.* **2005**, *17*, 4282.
- (16) Sasaki, T.; Ukyo, Y.; Kuroda, K.; Arai, S.; Saka, H. *J. Electron Microsc.* **2003**, *52*, 309.
- (17) Sasaki, T.; Ukyo, Y.; Suda, A.; Sugiura, M.; Kuroda, K.; Arai, S.; Saka, H. *J. Ceram. Soc. Jpn.* **2003**, *111*, 382.

lattice remains unaltered as in the pyrochlore, thus resulting the so-called κ phase.^{9,18} By contrast, if re-oxidized at high temperature ($T_{\text{reoxn}} \geq 1173$ K), its cationic sublattice would rearrange back to a random distribution.^{9,13}

Though a number of authors have discussed the role of the surface^{11,13,14} and bulk^{8,9,11,14,19} structural properties of thermally aged samples in the control of their reducibility, a well-sounded global description of the relationship existing between structure and redox behavior of ceria–zirconia mixed oxides is still lacking.¹⁴

To gain some further insight into these important questions, we have prepared two $\text{Ce}_{0.62}\text{Zr}_{0.38}\text{O}_2$ samples exhibiting significant differences in their structural and redox properties. In addition to the bare oxides, the corresponding supported Rh samples, with a low metal loading, 0.3 wt %, were also prepared and investigated.

The above-mentioned samples have been characterized by means of high-resolution electron microscopy (HREM) and a number of chemical techniques including temperature-programmed hydrogen reduction, hydrogen volumetric chemisorption, and oxygen storage capacity (OSC). The analysis of the results obtained from these studies have allowed us to draw a number of relevant conclusions helping us to rationalize the relationship existing between the surface and the bulk structural properties of the thermally aged ceria–zirconia mixed oxides and their redox response in both low- and high-temperature ranges.

Experimental Section

The ceria–zirconia mixed oxide samples investigated here have been prepared by applying to two aliquots of 25 g of a commercial, low surface area (S_{BET} , $19 \text{ m}^2 \cdot \text{g}^{-1}$) $\text{Ce}_{0.62}\text{Zr}_{0.38}\text{O}_2$ sample (CZ-LS), kindly provided by Grace Davison, a common reduction treatment consisting of heating, in a flow of pure hydrogen of $500 \text{ cm}^3 \cdot \text{min}^{-1}$, at $5 \text{ K} \cdot \text{min}^{-1}$, up to 1223 K, followed by 5 h of isothermal treatment at 1223 K; finally, the gas flow was switched to He ($500 \text{ cm}^3 \cdot \text{min}^{-1}$), for 1 h, and cooled to 298 K under inert gas flow. After completing this severe reduction (SR) step, the aging cycles were closed by applying to each of the aliquots a different re-oxidation routine. To prevent the overheating of the reduced mixed oxides, they were first re-oxidized at 298 K by pulsing O_2 (5%)/He until there was no evidence of further oxygen consumption; then, they were heated either in a flow of O_2 (5%)/He ($500 \text{ cm}^3 \cdot \text{min}^{-1}$), at 773 K for 1 h (mild oxidation (MO) step) or in a flow of pure O_2 ($500 \text{ cm}^3 \cdot \text{min}^{-1}$), at 1223 K for 5 h (severe oxidation (SO) step). The resulting oxide samples will be hereafter referred to as CZ-LS-SR-MO, in short CZ-MO (BET surface area, $16 \text{ m}^2 \cdot \text{g}^{-1}$), and CZ-LS-SR-SO, in short CZ-SO (BET surface area, $12 \text{ m}^2 \cdot \text{g}^{-1}$).

The corresponding 0.3% Rh/CZ-MO and 0.3% Rh/CZ-SO samples were prepared by incipient wetness impregnation of the corresponding oxides with an aqueous solution of $\text{Rh}(\text{NO}_3)_3$. After impregnation and drying in air, for 10 h, at 383 K, the resulting samples were calcined at 773 K for 1 h, cooled to 298 K under oxygen, and stored in a sealed flask until their use.

The temperature-programmed reduction mass spectrometry (TPR-MS) studies were performed in an experimental device coupled to

a quadrupole mass spectrometer, Pfeiffer, model QSM 200 M2. The amount of sample routinely used in these experiments was 200 mg, the 5% H_2/Ar flow rate was $60 \text{ cm}^3 \cdot \text{min}^{-1}$, and the heating ramp was $10 \text{ K} \cdot \text{min}^{-1}$. Prior to all the TPR runs, the samples were cleaned by heating them under flowing 5% O_2/He at $60 \text{ cm}^3 \cdot \text{min}^{-1}$, at a heating rate of $10 \text{ K} \cdot \text{min}^{-1}$, up to 773 K; then, they were kept for 1 h at this temperature and cooled to 398 K under the same flow of diluted oxygen and finally to 298 K in a flow of He.

The redox characterization of the investigated samples also included OSC measurements. To estimate the OSC values, two different approaches have been followed. In the most conventional one, usually referred to as ultimate OSC,²⁰ the experimental data were obtained from oxygen volumetric chemisorption. The isotherms were recorded on a Micromeritics, ASAP 2020, instrument. The oxygen partial pressure interval was 0–300 Torr, and the temperature was 473 K. The samples were pre-reduced in accordance with the following protocol: 400 mg was heated in a flow of 5% H_2/Ar ($60 \text{ cm}^3 \cdot \text{min}^{-1}$) at $10 \text{ K} \cdot \text{min}^{-1}$, from 298 K up to the selected reduction temperature (T_{redn}), was further kept at $T = T_{\text{redn}}$ for 1 h, under a flow of 5% H_2/Ar , then was evacuated for 1 h (residual pressure $< 1 \times 10^{-6}$ Torr) at $T_{\text{evac}} = T_{\text{redn}}$ or $T_{\text{evac}} = 773$ K if $T_{\text{redn}} \leq 773$ K, and finally was cooled to 473 K under high vacuum. These evacuation conditions ensure the elimination of any significant amount of hydrogen chemisorbed on the oxides. In the case of the supported Rh samples, the OSC values were determined by discounting from the total oxygen consumption the amount due to the rhodium re-oxidation to Rh_2O_3 . In accordance with the low Rh content of our samples, this correction represents less than 2% of the theoretical limit to be reached by the ceria–zirconia mixed oxide. It is assumed in this estimate that $\text{Ce}^{4+} \rightarrow \text{Ce}^{3+}$ is the only significant process.

The second type of OSC data to be discussed in this work will be referred to as instantaneous OSC. They were estimated by integration of the TPR traces up to some predefined time/temperature. Because the TPR experiments consisted of a heating ramp of $10 \text{ K} \cdot \text{min}^{-1}$ up to 1223 K, followed by a 1 h isothermal step at this temperature, the estimate of instantaneous OSC data was based on the assumption that the reduction degree deduced from the integration over the time of the overall TPR trace, with 1 h isothermal step at 1223 K included, corresponds to the ultimate OSC value at 1223 K. In fact, the reduction treatment is exactly the same in both experiments.

HREM images were recorded on a JEOL 2010-FEG instrument with a structural resolution of 0.19 nm. Electron microscopy specimens were prepared by depositing the samples to be investigated onto holey carbon coated 3 mm Cu grids. To avoid any contact with solvents, deposition was achieved by dipping the grids directly into the powder samples and further blowing off the excess.

The structural analysis of the recorded images has been performed by using the Digital Micrograph 3.4.3 suite. The experimental HREM images were digitized from negative plates using a KAPPA (1024×1024 , 12 bits) charge-coupled device camera. The digital diffractograms (DDPs) reported here correspond to the log-scaled power spectrum of the corresponding fast Fourier transforms.

Results and Discussion

HREM Study. Figure 1 shows representative HREM images of CZ-LS (A), CZ-SO (B), and CZ-MO (C) mixed oxides. Some significant differences may be noted between

(18) Kishimoto, H.; Omata, T.; Otsuka-Yao-Matsuo, S.; Ueda, K.; Hosono, H.; Kawazoe, H. *J. Alloys Compd.* **2000**, *312*, 94.
(19) Izu, N.; Kishimoto, H.; Omata, T.; Yao, T.; Otsuka-Yao-Matsuo, S. *Sci. Technol. Adv. Mater.* **2001**, *2*, 443.

(20) Duprez, D.; Descorme, C. In *Catalysis by Ceria and Related Materials*; Trovarelli, A., Ed.; Imperial College Press: London, 2002; Chapter 7, pp 243–280.

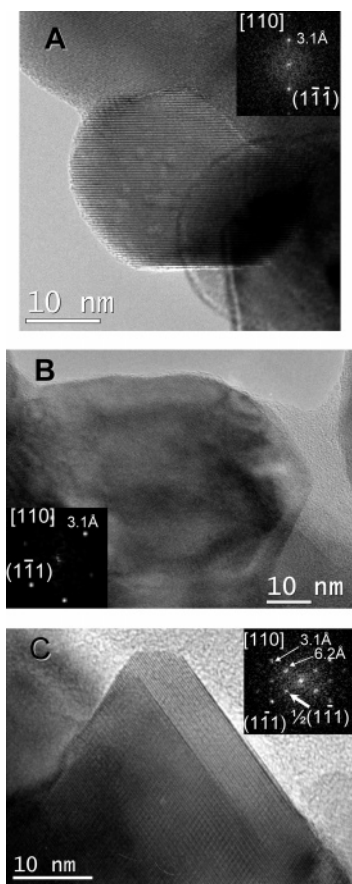


Figure 1. Representative high-resolution transmission electron microscopy images recorded for CZ-LS (A), CZ-SO (B), and CZ-MO (C) mixed oxide samples. The spots observed in the DDPs shown as insets have been indexed on the basis of the fluorite structure. $\frac{1}{2}(111)$ reflections at 6.2 Å are those characteristic of the pyrochlore-type superstructure.

CZ-MO (Figure 1C) and the remaining two samples, Figure 1A,B. As deduced from the analysis of HREM images such as the one reported in Figure 1C, the CZ-MO sample shows a very specific type of contrast characterized by a spatial frequency (lattice spacing) double as opposed to that observed in the LS sample. As recently discussed in refs 15–16, this structural feature, which cannot be found in the images recorded for the CZ-LS sample and is rarely observed in those of the CZ-SO oxide, is indicative of the characteristic ordering in the Ce–Zr sublattice observed in the pyrochlore-related κ phase. Likewise, the morphology of the oxide particles looks like very different, with rounded ill-defined facets in the LS and SO samples and a much better defined external shape, with an abundant presence of well-developed (111) faces, in the CZ-MO sample. The latter observation has been recently confirmed by a high angle annular dark field (HAADF) tomography study, in accordance with which the CZ-MO sample exhibits a significant number of microcrystals with almost perfect octahedron shape.²¹ Moreover, as discussed in ref 21, in the κ -like phase, because of the Ce–Zr sublattice ordering two sorts of (111) planes may be distinguished. One of them shows a Ce/Zr atomic ratio of 4:1, whereas the other one consists of a Zr-rich plane (Ce/

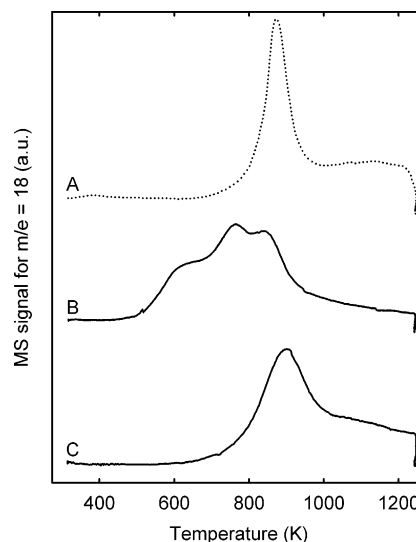


Figure 2. TPR-MS study of CZ-LS (A), CZ-MO (B), and CZ-SO (C) mixed oxide samples. Traces correspond to $m/e = 18$ (H_2O). Details of the whole protocol followed in these studies may be found in the experimental section.

Zr = 2:3). The detailed analysis of HAADF contrasts recorded for the CZ-MO sample has revealed that the preferentially developed (111) surface planes always correspond to zirconium-rich type.²¹

The analysis of Figure 1B shows that the SO treatment leading to the CZ-SO sample destroys the characteristic contrasts of the κ phase, thus suggesting that associated with it an order–disorder transition in the Ce–Zr sublattice occurs. As revealed by the profound effects on the external morphology of the oxide particles, the destruction of the κ phase very probably starts at the oxide surface. Accordingly, the CZ-MO and CZ-SO samples should be expected to exhibit significant differences in their structural and chemical surface properties.

The HREM study has also shown that, in the case of the CZ-SO, contrary to that noted for CZ-LS, some of the rest of the pyrochlore-related κ phase is still present in the sample. This is a noticeable observation because, very probably, this residual phase may favor the development of the κ phase in the case of applying further redox aging cycles to the sample.^{13,14}

TPR-MS and H_2 Chemisorption Studies on the Bare Oxide Samples. Figure 2 reports on the TPR-MS diagrams ($m/e = 18$, H_2O signal) recorded for the three ceria–zirconia mixed oxides, CZ-LS (A), CZ-MO (B), and CZ-SO (C). In good agreement with a number of earlier studies,^{8–11,13,14} the aging pretreatments applied to the fresh CZ-LS sample significantly modify its redox chemistry, the CZ-MO sample showing, as expected, an enhanced low-temperature reducibility with respect to that exhibited by CZ-LS and CZ-SO mixed oxides.

To better understand the origin of the differences observed in the TPR-MS traces reported in Figure 2A–C, we have investigated the hydrogen chemisorption on the CZ-MO and CZ-SO mixed oxide samples. The experiments consisted of heating them, for 30 min, under 38 Torr of hydrogen (the hydrogen partial pressure used in the TPR experiments), at increasing temperatures of 298, 373, 423, 448, and 473 K,

(21) Hernández, J. C.; Rodríguez-Luque, P.; Yeste, M. P.; Bernal, S.; Calvino, J. J.; Pintado, J. M.; Trasobares, S.; Hungría, A. B.; Midgley, P.; Pérez-Omil, J. M. Submitted for publication.

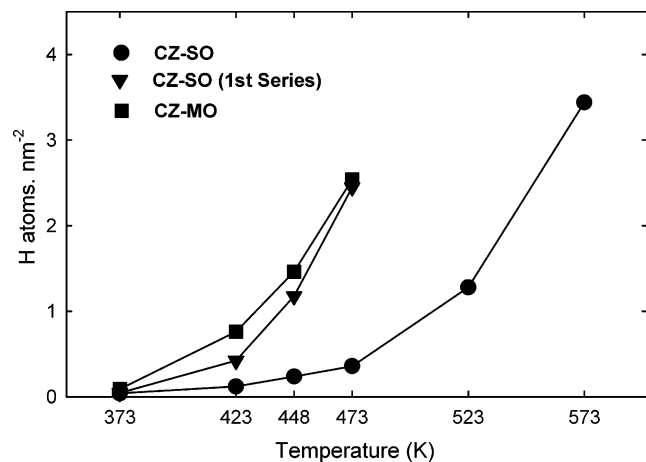


Figure 3. Volumetric study of hydrogen chemisorption on the $\text{Ce}_{0.62}\text{Zr}_{0.38}\text{O}_2$ samples. Initial hydrogen pressure: 38 Torr. The samples were submitted to successive cycles consisting of their heating at the indicated temperatures for 30 min followed by cooling to 298 K always under hydrogen. Pressure drops were determined at 298 K. CZ-SO (first series) accounts for the sample resulting from the first series of ultimate OSC measurements carried out on the CZ-SO sample.

followed in every case by cooling to 298 K under hydrogen pressure. The amount of chemisorbed hydrogen after each of these cycles was determined volumetrically, that is, from the decrease of P_{H_2} measured at 298 K. Figure 3 depicts the recorded data for both the CZ-SO and the CZ-MO samples. In accordance with earlier studies on the H_2 adsorption on ceria^{22,23} and ceria–zirconia,²⁴ the process implies the dissociation of the molecule with inherent formation of atomic chemisorbed species. Consistently, the quantitative data in Figure 3 are expressed as number of hydrogen atoms per squared nanometer. In accordance with the TPR-MS diagrams reported in Figure 2, the perturbation of the hydrogen chemisorption process by the simultaneous occurrence of oxide reduction, with inherent formation of H_2O , should be expected to represent a minor side effect.

Assuming that the H_2 consumption data reported in Figure 3 may be interpreted as due to atomic chemisorbed hydrogen, we may conclude that, for temperatures ranging from 373 to 473 K, the ability of CZ-MO for dissociating the hydrogen molecule is significantly higher than that of CZ-SO. In fact, in the range of temperatures mentioned above, the surface density of chemisorbed hydrogen is approximately six times larger on the CZ-MO sample. We may conclude that H_2 activation is much faster on the CZ-MO samples. The kinetic nature of the limitations observed in the H_2 adsorption on the CZ-SO sample was further confirmed by extending the heating–cooling cycles under H_2 up to 573 K, a temperature still below that at which the reduction of CZ-SO sample starts, Figure 2C. As shown in Figure 3, on CZ-SO, the amount of chemisorbed hydrogen progressively increases with the temperature, the value recorded at 573 K being even higher than that determined at 473 K for CZ-MO. These observations strongly suggest the relevance of the H_2

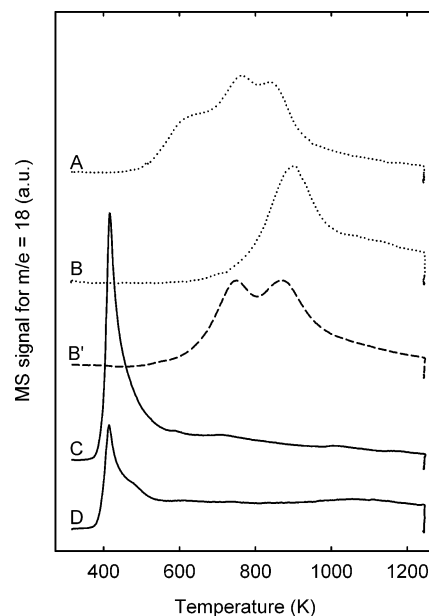


Figure 4. Influence of supported rhodium on the redox response of the ceria–zirconia mixed oxides. TPR-MS study. Traces corresponding to the $m/e = 18$ (H_2O) signal for CZ-MO (A), CZ-SO (B), 0.3% Rh/CZ-MO (C), and 0.3% Rh/CZ-SO (D) samples. Trace B' was recorded after applying the first series of ultimate OSC measurements to the CZ-SO sample. Details of the TPR protocol may be found in the experimental section.

chemisorption step in the control of the low-temperature reducibility of the mixed oxide samples.

TPR-MS Studies on the Oxide-Supported Rhodium Samples. To give some further support to the hypothesis advanced in the previous paragraph, we have carried out parallel redox studies on the corresponding rhodium-containing samples, 0.3% Rh/CZ-MO and 0.3% Rh/CZ-SO. Figure 4C,D reports respectively on the TPR-MS traces recorded for them. To facilitate the comparison, the diagrams for the bare oxides, CZ-MO (Figure 4A) and CZ-SO (Figure 4B) have also been included in this figure. As already noted in the experimental section, the contribution of Rh_2O_3 reduction approximately represents 2% of the overall area under the H_2O ($m/e = 18$) signals in Figure 4C,D.

The comparison of the TPR-MS traces for the bare oxides, Figure 4A,B, and the corresponding Rh-containing samples, Figure 4C,D, clearly shows that the supported metal phase dramatically enhances the low-temperature reducibility of both CZ-MO and CZ-SO mixed oxide samples. As presently well-established,^{24–26} in the presence of highly dispersed rhodium, an alternative, much faster mechanism of generating atomic hydrogen species on the oxide surfaces, the spillover, becomes operative. Consequently to this, the kinetic limitations for hydrogen chemisorption on the bare oxides are overcome, and a very significant increase of their reduction rate occurs. This would explain the strong downward shifts observed in the main peaks of the TPR-MS diagrams for the supported rhodium samples, 350 K in the case of the CZ-MO sample, and as much as 500 K in the case of the CZ-SO one. Di-hydrogen activation would thus constitute

(22) Bernal, S.; Calvino, J. J.; Cifredo, G. A.; Rodríguez-Izquierdo, J. M.; Perrichon, V.; Laachir, A. *J. Catal.* **1992**, *137*, 1.

(23) Bernal, S.; Calvino, J. J.; Cifredo, G. A.; Rodríguez-Izquierdo, J. M. *J. Phys. Chem.* **1995**, *99*, 11794.

(24) Norman, A.; Perrichon, V.; Bensaddik, A.; Lemaux, S.; Bitter, H.; Koningsberger, D. *Top. Catal.* **2001**, *16/17*, 363.

(25) Hickey, N.; Fornasiero, P.; Kaspar, J.; Gatica, J. M.; Bernal, S. *J. Catal.* **2001**, *200*, 181.

(26) Gatica, J. M.; Baker, R. T.; Fornasiero, P.; Bernal, S.; Blanco, G.; Kaspar, J. *J. Phys. Chem. B* **2000**, *104*, 4667.

Table 1. OSC Data Expressed as Percentage of Total Ce⁴⁺ Reduced to Ce³⁺

sample/reducing atmosphere	ultimate OSC (%) at $T(K)^a$ (volumetric adsorption of O ₂)					instantaneous OSC (%) ^b (integration of TPR diagrams)							
	473 K	623 K	773 K	973 K	1173 K	1223 K	473 K	623 K	773 K	973 K	1173 K	1223 K	1223 K (1 h) ^c
CZ-LS/ 5% H ₂ /Ar		4	30	44	61	70	0	0	2	37	55	61	70
CZ-MO/ 5% H ₂ /Ar	8	45	63	74	83	82	1	10	37	68	78	79	82
Rh/CZ-MO/ 5% H ₂ /Ar	45	54	65	75	81	82	32	49	58	68	75	77	82
CZ-SO/ 5% H ₂ /Ar	0	3	17	50	62	69	0	1	4	38	56	59	69
CZ-SO/ 5% H ₂ /Ar ^d		15	45			70	0	2	20	50	63	65	70
Rh/CZ-SO/ 5% H ₂ /Ar	23	31	39		67	71	13	25	34	46	59	65	71

^a Ultimate OSC data as determined by oxygen volumetric isotherms (final P_{O_2} , 300 Torr) at 473 K. Experiments carried out on 400 mg of samples pre-reduced as follows: heating in a flow of 5% H₂/Ar (60 cm³·min⁻¹), at 10 K·min⁻¹, from 298 K to the selected temperature (T_{redn}), further kept at $T = T_{redn}$, for 1 h, under flow of 5% H₂/Ar, then evacuated for 1 h (residual pressure $< 1 \times 10^{-6}$ Torr), at $T_{evac} = T_{redn}$ or $T_{evac} = 773$ K for $T_{redn} \leq 773$ K, and finally cooled to 473 K under high vacuum. In the case of Rh-containing samples, the OSC values were corrected by taking into account the contribution of Rh re-oxidation to Rh₂O₃ to the total oxygen consumption. ^b Instantaneous OSC data as determined by integration of the TPR-MS signal for $m/e = 18$ (H₂O) up to the selected temperature. Experimental conditions in the TPR-MS runs: amount of sample, 200 mg; 5% H₂/Ar flow rate, 60 cm³·min⁻¹; heating rate, 10 K·min⁻¹. Top limit temperature: 1223 K. Time at 1223 K: 60 min. ^c OSC values corresponding to the overall TPR experiment including 1 h of isothermal reduction at 1223 K. Data used as reference values for estimating the instantaneous OSC at the different temperatures. It is assumed to agree with the corresponding ultimate OSC values at 1223 K. ^d Second series of ultimate OSC measurements after completing the first one.

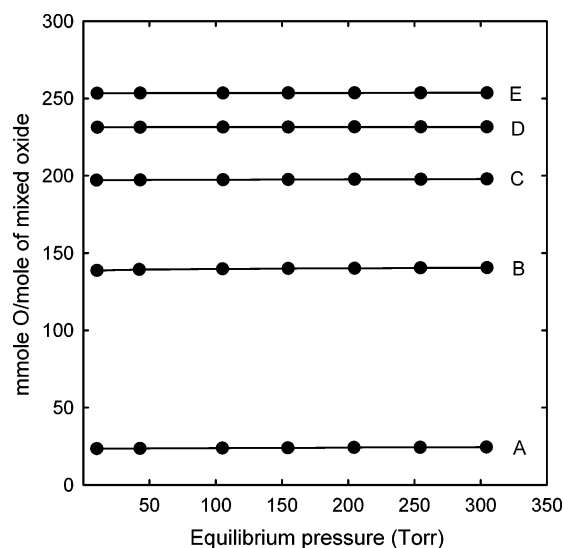


Figure 5. Series of O₂ volumetric isotherms recorded at 473 K for the CZ-MO sample reduced at 473 (A), 623 (B), 773 (C), 973 (D), and 1223 K (E). Details of the reduction/evacuation protocol applied in this study may be found in the experimental section.

the rate controlling step in the overall reduction process of the bare oxides. Moreover, as already shown in Figure 3, the different low-temperature reducibility exhibited by the bare CZ-MO and CZ-SO samples is fully consistent with their different ability to activate the hydrogen chemisorption, which in turn supports the significant difference in their surface chemistry already suggested by the analysis of the HREM images.

OSC Measurements. The study of the OSC of the ceria–zirconia samples has also provided some additional, very interesting, pieces of information. As established in the experimental section, two types of OSC data will be considered here, ultimate and instantaneous OSC.

Regarding the ultimate OSC measurements, Figure 5 shows the series of oxygen isotherms recorded at 473 K for the bare CZ-MO sample reduced at temperatures ranging from 473 to 1223 K. As deduced from the shape of the recorded isotherms, with independence of the pre-reduction temperature, oxygen chemisorption at 473 K is very fast and strong, leading to the complete re-oxidation of the samples at the very first point; that is, at the lowest of the investigated O₂ partial pressures. Despite this evidence, it was checked

that no further oxygen uptakes occurred upon increasing the re-oxidation temperature at 573 K and even 673 K, under 300 Torr of oxygen. The shape of the isotherms recorded for CZ-SO, Rh/CZ-MO, and Rh/CZ-SO looked very similar to those reported in Figure 5.

On the basis of these volumetric re-oxidation studies, we have determined the ultimate OSC data reported in Table 1 for all the investigated samples, with and without rhodium. As detailed in the experimental section, prior running the O₂ isotherms, the samples were reduced with flowing 5% H₂/Ar for 1 h, at temperatures ranging from 473 to 1223 K, and further evacuated at either 773 K or T_{redn} , if the latter was higher than 773 K.

The instantaneous OSC data, which are also included in Table 1, were estimated by integrating the TPR traces in Figures 2 and 4 as indicated in the experimental section.

Regarding the results reported in Table 1, there are a number of interesting points to be commented on. In good agreement with the TPR-MS results, the ultimate OSC data, in particular those recorded for $T_{redn} \leq 773$ K, clearly show that the presence of Rh very much enhances the reducibility of both CZ-MO and CZ-SO samples. Therefore, in the low-temperature region, the OSC values reported for the bare oxides do not represent true equilibrium situations. This effect is particularly noticeable on the CZ-SO oxide, for which, even at 773 K, the difference between the ultimate OSC values recorded with and those recorded without rhodium is still very significant, 17% for the bare oxide and 39% for the supported rhodium sample. This observation suggests that, to obtain meaningful low-temperature ultimate OSC values, the study of supported rhodium samples, instead of the bare oxides, constitutes the best experimental option. Otherwise, the OSC values for $T_{redn} \leq 773$ K would certainly be determined by kinetic rather than thermodynamic factors.

At the highest T_{redn} values, on the contrary, the influence of rhodium becomes much less significant, thus suggesting that the ultimate OSC data for the bare oxides are close to the equilibrium values. Accordingly, the ultimate OSC determined for CZ-MO and CZ-SO at $T_{redn} \geq 973$ K may be considered as indicative of the existence of an intrinsic thermodynamic difference between them, the CZ-MO sample showing a higher reducibility than the CZ-SO one. This conclusion is in agreement with a number of earlier studies

from the literature,^{12,19,27} being also consistent with the low-temperature OSC values reported in Table 1 for the rhodium-containing samples, as well as with the shape of the TPR-MS diagrams depicted in Figures 4C (Rh/CZ-MO) and 4D (Rh/CZ-SO).

Also remarkable, the high-temperature ultimate OSC data in Table 1 indicate a close redox behavior for the CZ-LS and CZ-SO samples. This resemblance reinforces the likely existence of a relationship between ordering in the cationic sublattice and thermodynamic reducibility of the corresponding oxide samples.¹⁹

By using as a reference the (111) plane of the corresponding pseudo-fluorite structure and assuming that the highest surface reduction degree is the same as the one resulting for the fully reduced oxide, we have estimated that a purely surface reduction process represents less than 5% of the total reduction degree of our CZ-SO and CZ-MO samples. Therefore, in the presence of supported Rh, at 473 K, the ultimate OSC data are far larger than those corresponding to a purely surface process. We should conclude, accordingly, that even at such a low temperature, diffusion of surface vacancies into the bulk of both CZ-SO and CZ-MO oxide samples is fast enough as not to represent the controlling step in the kinetics of the overall reduction process. This observation is in agreement with some earlier studies on the redox behavior of ceria–zirconia mixed oxides, in accordance with which the incorporation of zirconia into the ceria lattice strongly promotes its bulk reduction.^{28–30} Likewise, it is consistent with the high oxygen mobility deduced from a number of electric conductivity measurements carried out on different ceria–zirconia mixed oxides.^{19,30} The low-temperature instantaneous OSC data reported in Table 1 do also support this statement.

Regarding the high-temperature data reported in Table 1 for the CZ-SO sample, there is an additional major point to be commented on. As is known,⁹ at high temperature, under reducing conditions, the random distribution of Ce and Zr in the CZ-SO lattice becomes unstable against ordering with subsequent creation of a pyrochlore type cationic sublattice. Consequently, for the reduced CZ-SO state, the occurrence of a cationic rearrangement leading to the corresponding reduced form of the CZ-MO phase would be favored. The different ultimate OSC values reported in Table 1 for CZ-SO and CZ-MO samples reduced with 5% H₂/Ar for 1 h at 1223 K, 82% and 71%, respectively, would, therefore, indicate that the kinetics of the cationic sublattice rearrangement is slow enough as to allow us the use of ultimate OSC data at 1223 K as a chemical marker of the structural properties, in particular of the cationic sublattice ordering, in the ceria–zirconia sample.

In accordance with the available literature,^{10,11,13,14} however, the reduction treatment at 1223 K applied in our

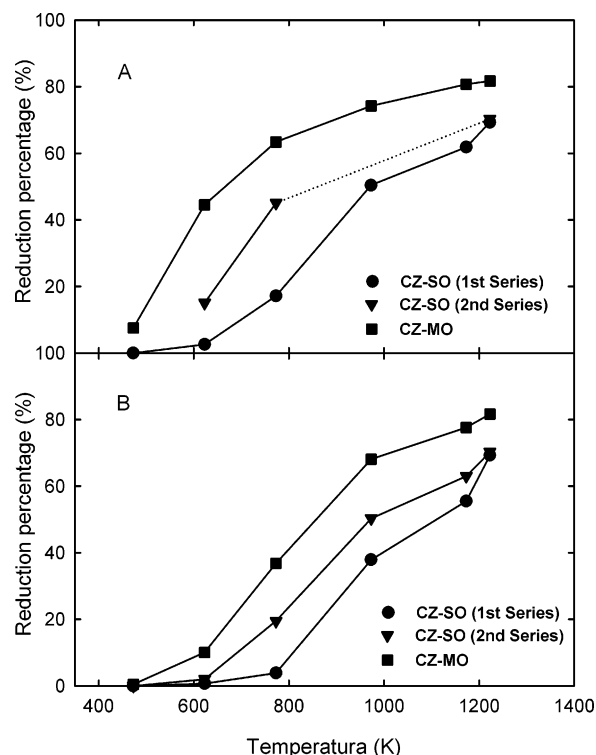


Figure 6. Variation with the temperature of ultimate (A) and instantaneous (B) OSC data for CZ-MO, CZ-SO (first series), and CZ-SO (second series). See Table 1 and the experimental section for further details about the way of obtaining the OSC values.

ultimate OSC measurements should be expected to significantly enhance the reducibility of the CZ-SO sample. Likewise, HREM and HAADF studies¹⁶ carried out on a ceria–zirconia sample treated under conditions similar to those applied in the OSC experiments mentioned above have shown the occurrence of a κ -like phase. Despite this, a significant difference is observed between the OSC data at 1223 K for CZ-MO and CZ-SO samples. To clarify this important point, we run an additional series of ultimate OSC measurements on the CZ-SO sample resulting from the first series. Table 1 and Figure 6 summarize the corresponding results. A remarkable observation can be made. As expected,^{10,11,13,14} in the second series, the OSC values determined at 623 K (OSC, 15%) and 773 K (OSC, 45%) are much larger than those obtained in the first one, 3% and 17%, respectively. On the contrary, data at 1223 K are much closer, 69% in the first series and 70% in the second one. If we assume that the latest OSC values account for the bulk thermodynamic properties of the CZ-SO oxide reduced at 1223 K, we should conclude that no substantial modification of them has been induced by the first series of OSC measurements. This contrasts with the larger OSC value recorded at 1223 K for CZ-MO. The atmosphere, pure hydrogen instead of 5% H₂/Ar, and the duration of treatment, 5 h instead of 1 h, would explain the difference of bulk thermodynamic properties between cycled CZ-SO and CZ-MO samples. The enhancement of low-temperature reducibility deduced from the second series of OSC measurements carried out on the CZ-SO sample should, therefore, be conciliated as a mainly a kinetic effect.

To consolidate all the observations made in the previous paragraphs we propose, as already hypothesised,^{13,14} that the

- (27) Izu, N.; Kishimoto, H.; Omata, T.; Ono, K.; Otsuka-Yao-Matsuo, S. *Sci. Technol. Adv. Mater.* **2001**, *2*, 397.
 (28) Fornasiero, P.; Di Monte, R.; Ranga Rao, G.; Kaspar, J.; Meriani, S.; Trovarelli, A.; Graziani, M. *J. Catal.* **1995**, *151*, 168.
 (29) Vidal, H.; Kaspar, J.; Pijolat, M.; Colon, G.; Bernal, S.; Cordon, A.; Perrichon, V.; Fally, F. *Appl. Catal., B* **2001**, *30*, 75.
 (30) Boaro, M.; Trovarelli, A.; Hwang, J. H.; Mason, T. O. *Solid State Ionics* **2002**, *147*, 85.

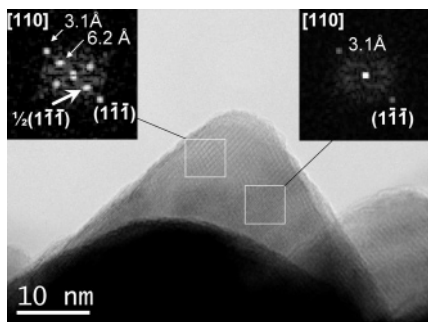


Figure 7. High-resolution transmission electron microscopy study of the oxide resulting from the application to the CZ-SO sample of a treatment similar to the one used for determining the first series of OSC data. DDPs corresponding to two different regions of the crystallite are shown as insets. The reported spots have been indexed on the basis of the fluorite structure. $\frac{1}{2}\{111\}$ superstructure reflections at 6.2 Å are clearly observed in the DDP of the region closer to the surface. Note also the rough and rounded appearance of the crystallite surface.

reduction at 1223 K and further re-oxidation treatment applied to CZ-SO during the OSC measurements would essentially induce some surface regeneration of the κ -like phase. Though this phase may not be relevant in quantitative terms, if localized on the surface of the oxide, it may play an important kinetic role in the hydrogen chemisorption step. In fact, as deduced from Figure 3, the capability of this sample for low-temperature activation of H_2 , though lower than that of the CZ-MO sample, is higher than that exhibited by CZ-SO. Consistently, its TPR diagram, Figure 4B', does also show that the oxide reduction starts at an intermediate temperature between those observed for the CZ-SO and CZ-MO samples. Though less efficiently, the surface κ phase would play a role similar to that of the supported rhodium. It would modify the kinetics of the H_2 dissociation, thus making faster the low-temperature reduction of the mixed oxide. In quantitative terms, however, the contribution of the κ phase to the overall thermodynamic properties of the oxide sample would be small enough as not to significantly modify the ultimate OSC value at 1223 K.

In addition to the chemical studies commented on above, the CZ-SO sample resulting from the first series of OSC measurements has also been investigated by means of HREM. Figure 7 shows one of the recorded images. A micrograph of similar characteristics for the CZ-MO sample is reported in Figure 1C. At first glance, the external shapes of the particles shown in Figures 7 and 1C look rather similar. This analogy may be considered as a qualitative indication of the surface development of the κ phase in the CZ-SO sample resulting from the first series of OSC measurements. In fact, the high-resolution image in Figure 7 unequivocally shows the super-structure contrasts with lattice spacing twice that observed in the fluorite-like structure which characterizes the κ phase. Likewise, the DDP included as an inset in Figure 7 confirms the regeneration of the κ phase and the analogies observed between Figures 7 and 1C. Some remarkable differences may be noted, however, between these HREM images. First, as confirmed by the DDP insets, in the cycled CZ-SO sample the characteristic contrasts of both the κ -like phase and the one corresponding to the disordered cationic sublattice, Figure 7, do coexist. Moreover, the comparison of Figures 7 and 1C suggests some differences in the external

morphology of the oxide particles, the microcrystal profiles of the CZ-MO sample showing much more sharply defined (111) facets. We should conclude, accordingly, that, as expected, the rearrangement of the cationic sublattice leading to the formation of the κ phase and inherent development of well-faceted microcrystals is slow enough as not to be completed in the CZ-SO sample resulting from the first series of OSC measurements. These very subtle differences, however, may be relevant in chemical terms. They suggest the existence of structural and compositional differences at the surface of the cycled CZ-SO and CZ-MO samples which may lead to a distinct capability for activating the di-hydrogen molecule.

Concluding Remarks

The results presented and discussed in this work show that the temperature of re-oxidation applied to a heavily reduced ceria–zirconia sample induces both thermodynamic and kinetic effects on the redox behavior of the resulting samples. High-temperature re-oxidation leads to a mixed oxide, CZ-SO sample, whose reduction is slower and less thermodynamically favored than that of the CZ-MO one. Our results do also support that, in the low-temperature region ($T \leq 773$ K), though the intrinsic thermodynamic difference between CZ-MO and CZ-SO samples does exist, their redox response is mainly governed by kinetic factors related to a different surface chemistry. In particular, as suggested by the dramatic effect of the supported rhodium, di-hydrogen activation is most likely the rate determining step in their overall reduction process.

The thermodynamic differences of reducibility between the CZ-MO and the CZ-SO samples may be rationalized by considering that, under oxidizing conditions, the phase resulting from a mild re-oxidation of the pyrochlore-related κ -like phase (CZ-MO sample) is not stable against the transition order–disorder in its cationic sublattice; that is, the so-called κ phase represents a meta-stable thermodynamic state.²⁷ Accordingly, the reduction of the CZ-MO sample corresponds to the transformation of the meta-stable initial state, the κ phase, into the most stable final reduced state, the pyrochlore-like phase. For the CZ-SO sample, on the contrary, the initial state corresponds to an oxidized sample with a random distribution of Ce and Zr ions, that is, the most stable one, whereas the final state is associated with a reduced oxide with a disordered cationic sublattice, a meta-stable situation with respect to that of the pyrochlore-like ordered phase.

An in-depth understanding of the kinetic differences observed in the low-temperature reducibility of CZ-MO and CZ-SO samples would certainly require further studies on the structural and electronic properties of the mixed oxide surfaces, as well as on the mechanism of the di-hydrogen activation on them. Nevertheless, it should be stressed that, as deduced from the combination of HREM and chemical studies reported here, the appearance of the κ phase does also imply the creation of surface structures highly active against hydrogen activation, which in turns constitutes the rate controlling step in the low-temperature reduction of the ceria–zirconia mixed oxides.

Finally, it must be recalled that, very often, as shown in this work, the applied thermo-chemical aging treatments do not lead the ceria–zirconia systems to true equilibrium states. Consequently, compositionally and structurally inhomogeneous samples may result.^{13,31} This circumstance very much complicates a detailed interpretation of the effects of thermal aging on the redox chemistry of a specific oxide sample, as well as the comparative analysis of data from different authors. Despite these limitations, there is a general agreement on the nature of the chemical and structural effects induced on the ceria–zirconia mixed oxides showing the tetragonal structure by thermal aging pretreatments similar to those applied here.² In this work, significant progress has been made in the correlation of thermal aging conditions, nanostructural properties of the resulting oxides, and relevance of the thermodynamic and kinetic factors in the control of the observed changes of reducibility. As deduced from the results presented and discussed here, depending on the temperature, hydrogen partial pressure, and time of treatment applied during the reduction step of the aging cycle, the ordering induced in the Ce–Zr cationic sublattice would affect either limited regions of the sample, mainly localized at its surface, or the bulk of the oxide with variable, but significant, extent.

In the first case, the best technique for detecting the presence of a κ -like phase would certainly be HREM,¹⁶

whereas the most conventional, macroscopic ones such as X-ray diffraction or Raman spectroscopy, may be useless.^{13,14} Consistently, the parallel chemical effect, that is, the enhancement occurring in the reducibility of the oxide, would mainly have a kinetic origin. In contrast, the bulk thermodynamic properties of the oxide would remain unaltered. A representative example might well be the oxide resulting from the application the first series of ultimate OSC measurements to the CZ-SO sample.

In the second case, because of the much larger extent of the disorder–order transition undergone by the cationic sublattice, both thermodynamic and kinetic effects would be observed. In parallel with this, the quantitative weight of the κ -like phase would be much larger, and consequently its detection by X-ray diffraction or Raman spectroscopy would be easier.^{12,13,17,18} This situation would be typically associated with hard reduction conditions.^{12,13,17,18} The CZ-MO sample prepared in this work might be included in this category.

Acknowledgment. We acknowledge the financial support from the Ministry of Education and Science of Spain and the FEDER Program of the EU (Project No. MAT2005-00333) and the *Junta de Andalucía* (Groups FQM-110 and FQM-334). The ceria–zirconia mixed oxide sample was kindly donated by Grace Davison Company. HREM images were recorded at the Electron Microscopy facilities of the University of Cádiz.

CM0606351

(31) Mamontov, E.; Brezny, R.; Koranne, M.; Egami, T. *J. Phys. Chem. B* **2003**, *107*, 13007.